ADVANCED ENGINEERING MATERIALS
www.aem-journal.com

Surface Textures Fabricated by Laser Surface Texturing and Diamond Cutting – Influence of Texture Depth on Friction and Wear

Jun-Jie Zhang, Jian-Guo Zhang, Andreas Rosenkranz, Xiao-Li Zhao, and Ye-Lin Song*

In the present work, the authors study the tribological characteristics of textured stainless steel surfaces with different texture depths ranging from 1.3 to 23 μm created by laser surface texturing and ultra-precision diamond cutting. The periodicity of the surface textures is kept constant at 90 μm for each fabrication technique and texture depth. Subsequent ball-on-disk friction tests show that friction and wear can be effectively reduced by the surface texturing. It is found that the effectiveness of the surface textures greatly depends on the depth and the geometry of the textures, as well as on testing parameters such as the applied load and the sliding velocity. Surface textures with the lowest depth demonstrate a slightly increased COF as well as an increased mass loss under low loads or sliding velocities. On the other hand, surface textures with intermediate depths show a significant reduction in the COF and wear. The observed friction and wear reduction can be mainly attributed to a combined effect of the surface textures consisting of the generation of an additional hydrodynamic pressure, the storage of produced wear particles as well as the action as secondary source for lubricant (reservoir effect).

1. Introduction

With the continuously growing demand for energy saving and improved material consumption, the reduction of friction and wear in tribological components is essential. While friction reduction by an improved surface finish is ultimately restricted by complex material-oriented removal processes, surface texturing has become an effective method of surface treatment to improve the tribological performance of mechanical components. Numerous theoretical and experimental work have demonstrated that the friction reduction induced by surface texturing is a combined result of different mechanisms. For lubricated contacts, the additional hydrodynamic pressure can be named, thus leading to an increase of load-bearing capacity. On the other hand, surface textures can act as efficient traps for wear debris or induce a secondary oil supply based upon a reservoir effect.[1–6] In addition, surface textures can significantly reduce the real contact area, which leads to a reduced frictional force and coefficient of friction (COF).[7,8] Furthermore, it was found that the effect of surface texturing on friction reduction greatly depends on structural parameters such as area density, periodicity and depth as well as the texture's geometry and experimental conditions.[9–15]

Apart from the resulting tribological properties, remarkable attention has been paid to the fabrication of surface textures. Various techniques, such as electrochemical methods,[16–18] etching,[19] laser beam texturing,[20–24] abrasive jet machining,[25] engraving,[26] electrical discharge machining,[27,28] hot micro-coining,[29] and CNC machining,[30,31] have been successfully employed to fabricate surface textures to enhance the friction and wear behavior. It has been demonstrated that the resulting tribological properties also depend on the texturing technique used due to different machining characteristics.[32] Wakuda et al. utilized laser beam machining and abrasive jet machining to fabricate micro-dimples with the same size on silicon nitride mated with hardened steel. Their subsequent sliding tests showed that the dimple's morphology has a strong influence on the resulting friction reduction, which also depends on the sliding velocity. A more pronounced effect was verified for larger dimple diameters.[25]

The impact of the machining characteristic on the fabricated textures becomes more pronounced with decreasing feature

Dr. J.-J. Zhang
Center for Precision Engineering, Harbin Institute of Technology, Harbin 150001, China
E-mail: zhjj505@gmail.com
Dr. J.-G. Zhang
Department of Mechanical Science and Engineering, Nagoya University, Nagoya 464-8603, Japan
Changchun Institute of Optics, Fine Mechanics and Physics, Chinese Academy of Science, Changchun 130033, China
Dr. A. Rosenkranz
Center for Memory and Recording Research, University of California San Diego, La Jolla 92093, United States
Dr. X.-L. Zhao
School of Mechatronics Engineering, Harbin Institute of Technology, Harbin 150001, China
Y.-L. Song
School of Mechanical Engineering, Shanghai Jiao Tong University, Shanghai 200240, China

DOI: 10.1002/adem.201700995

size. The fabrication of very shallow textures with feature sizes in the submicron range, while maintaining the machining accuracy, is challenging for existing texturing techniques. For instance, the depth of textures fabricated by laser surface texturing is restricted by both the laser beam parameters and the texture geometries. On the other hand, ultra-precision diamond cutting is a promising technique to efficiently fabricate sophisticated surface micro-/nanostructures with high machining accuracy and feature sizes ranging from the nano-to micrometer scale.[33–35] Stainless steel is one of the most commonly used industrial materials for machine tool elements, and the tribological behavior of the working surface has a significant influence on the moving accuracy and the working life time of the machine tool. Consequently, it exists a great desire to reduce friction and wear in mechanical components made of stainless steel.

In the present work, we fabricate surface textures with depths ranging from 1.3 to 23 μm on SUS420J2 stainless steel by using two texturing methods, namely laser surface texturing and diamond cutting. In particular, for the smallest depth of 1.3 μm produced by diamond cutting, two texture geometries (square and sinusoidal) are realized. Subsequent ball-on-disk friction tests show that friction can be effectively reduced by the as-fabricated textures.

2. Methods

2.1. Laser Surface Texturing

Laser surface texturing is done by using a picosecond laser DL6000PU (DCT Co., Ltd., Tianjin, China) with a wavelength of 355 nm and a pulse duration of 9 ps. In this study, textures in the form of well aligned grooves with a periodicity of 90 μm are fabricated. The minimum depth h_{min} and maximum depth h_{max} of the surface textures are determined using the laser parameters and the texture geometries, which can be expressed by Equation 1 and 2:

$$N_1 = \frac{\Delta N}{h_{min}} \quad (1)$$

$$N_2 = \frac{2ah_{max}}{\lambda/2} \quad (2)$$

in which, N_1 is the deviation of texture depth, N_2 is the differential ratio between valley and crest widths of textures, ΔN is the laser machining accuracy, and a is the conical degree of the laser beam. In our case, ΔN is 0.5 μm and a is about 5%. Consequently, with the requirement that both N_1 and N_2 are smaller than 10%, four texture depths namely, 8, 13, 18, and 23 μm are selected. For each texture depth, the texture density is kept constant at 50%, and all laser parameters are kept constant (fixed power of 12 W, fixed laser fluence of 12.7 J cm^{-2} and fixed frequency of 1200 KHz). For laser surface texturing, multiple overpasses of the laser are needed in order to reach the nominal texture depth, that is, the textures are fabricated in a layer-by-layer fashion. Consequently, the manufacturing times are longer for higher texture depths. Specifically, the number of necessary overpasses to achieve texture depths of 8, 13, 18, and 23 μm are 5, 8, 24, and 30, respectively. The machining speed is 1000 and 1800 mm s^{-1} for low (8 and 13 μm) and high (18 and 23 μm) texture depths, respectively. After laser surface texturing, the textured surfaces are imaged by a large depth-of-field optical microscope, which also provides detailed information about the texture depth by cross-section profiles. Furthermore, the texture surfaces are imaged by a scanning electron microscope (SEM) to provide detailed information of local surface morphology.

Figure 1a shows an optical image of the as-fabricated surface texture with a depth of 18 μm by a large depth-of-field optical microscope. In addition, Figure 1b presents the corresponding cross-section profile measured over several individual texture units. It can be seen that although the alignment of fabricated groove structures is regular, the form accuracy is not perfectly uniform since there are some slight differences in the bottom morphologies of neighbored grooves. This can be induced by inaccuracies coming from the laser processing. Furthermore, Figure 1a shows that the bottom morphology is significantly changed compared to the untextured reference surface, that is, some thermal damage occurs in the valleys, which can be well correlated with the used pulse duration for the laser ablation. It is well known that a laser pulse duration in the order of 10 ps defines an important threshold with respect to the underlying laser-matter interaction. For pulse duration above 10 ps, the laser-matter interaction is typically based upon photo-thermal processes involving melting and resolidification phenomena. In

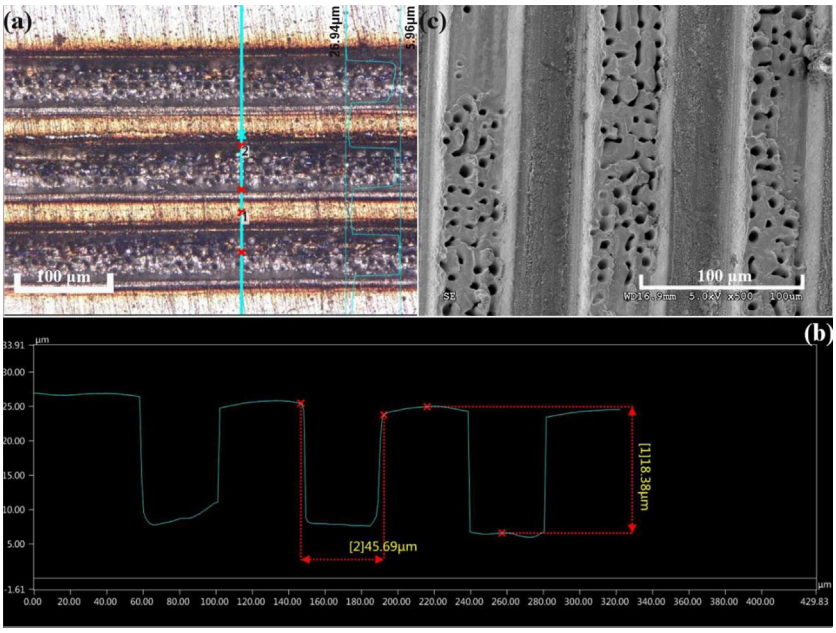

Figure 1. Laser surface texturing with a texture depth of 18 μm. a) Optical image; b) cross-section profile plot; and c) SEM micrograph.

contrast to that lasers with pulse durations below 10 ps are generally classified as ultra-short pulse laser systems and are based upon ablation. This correlates very well with the micrographs and profiles presented in Figure 1 since no bulges or rims can be found. Consequently, the thermal impact on the material during laser surface texturing is reduced. The fact that the thermal impact is not completely negligible when using laser with this pulse duration shows the SEM micrograph in Figure 1c. In this figure some recast phenomena occurring in the valleys due to thermal effects involved in picosecond laser ablation can be observed. It is worth to emphasize that the observed recast phenomena are more pronounced for larger texture depths due to longer processing times. Additionally, it is worth to emphasize that a further analysis of the surface chemistry and microstructure after laser texturing can be beneficial since the thermal impact can change the chemical and mechanical properties of the material. A detailed characterization and the connection with the resulting tribological properties will be subject of a follow-up study.

2.2. Ultra-Precision Diamond Cutting

Direct diamond cutting of stainless steel by a diamond cutting tool is challenging due to significant thermal diffusion between carbon and iron, which can lead to severe thermochemical tool wear that deteriorates machining accuracy. In the present work, surface textures with the lowest depths of 1.3 μm are fabricated using the elliptical vibration diamond cutting. As illustrated in **Figure 2**a, the elliptical vibration diamond cutting is an intermittent cutting process, in which the formed chip is pulled out in each vibration cycle to efficiently decrease the chip thickness and cutting force. Furthermore, thermal diffusion between the diamond cutting tool and the steel workpiece is significantly suppressed to prevent tool wear. At the same time, by precisely controlling the vibration amplitude in depth of cutting direction, the envelope of cutting edge trajectory can be precisely transferred into the machined surface, which leads to the successful fabrication of micro/nanostructures.[36,37] It should be mentioned that the curvature radius of the vibration locus is smaller than the minimum curvature radius of the target structures to avoid undesirable over-cutting.

Figure 2b and c show two different texture geometries, namely square and sinusoid, fabricated on stainless steel using elliptical vibration diamond cutting with a vibration frequency of 41.6 kHz. The textured surfaces are imaged by a white light interferometry, which provides detailed information related to the texture depth. The vibration amplitude in cutting direction is kept constant at 2 μm. On the other hand, the vibration amplitude in the depth of the cutting direction is changed from 0.7 to 2 μm with a frequency of 100 Hz. Finally, square and sinusoidal textures are successfully fabricated with the same depth of 1.3 μm. In order to be consistent with the surface textures fabricated by laser surface texturing, both geometries have a periodicity of 90 μm in cutting direction. For each texture geometry, the texture density and pitch are kept constant at 50% and 150 μm, respectively. It can be seen from Figure 2b and c that both geometries exhibit uniform characteristics with long-range order and high form accuracy.

2.3. Ball-on-Disk Tests

Unidirectional ball-on-disk friction tests are performed on a Bruker CTER-UMT-3 tribometer. A 9Cr18 steel ball with a diameter of 4 mm is used as a counter body rubbing against a SUS420J2 stainless steel specimen, as illustrated in **Figure 3**. The hardness of the counter body and the specimen is about 62 and 53 HRC, respectively. The respective tensile strength of the counter body and the specimen is about 1400 and 540 MPa, respectively. To achieve specimen rotation, a S24LE rotation unit with a maximum rotation speed of 4000 rpm and a load capacity of 20 kg was utilized. The track diameter in the friction tests was 16 mm. The friction force and normal load during the friction tests were measured by a force sensor. Consequently, the COF, defined as the ratio of friction force divided by the normal load after running-in, can be estimated. Seven sliding velocities between 4 and 28 m min^{-1} and four different normal loads, namely 4, 8, 12, and 16 N, are used for the friction tests in order to evaluate the tribological performance of the fabricated surface textures.

The SUS420J2 stainless steel is selected as the specimen material because of its superior wear resistance, strength, and hardness. The specimen has dimensions of 25, 25, and 10 mm in length, width, and depth, respectively. Prior to surface texturing, the specimens are grinded to obtain a surface roughness Ra of 0.1 μm. A commercial lubricant oil (Mobil 15W-40) with a dynamic viscosity of 13.3 $mm^2 s^{-1}$ and a density of 0.8678 kg l^{-1} at 30 °C is used for the friction tests under atmospheric pressure and at room temperature. Two hours before each test, an oil

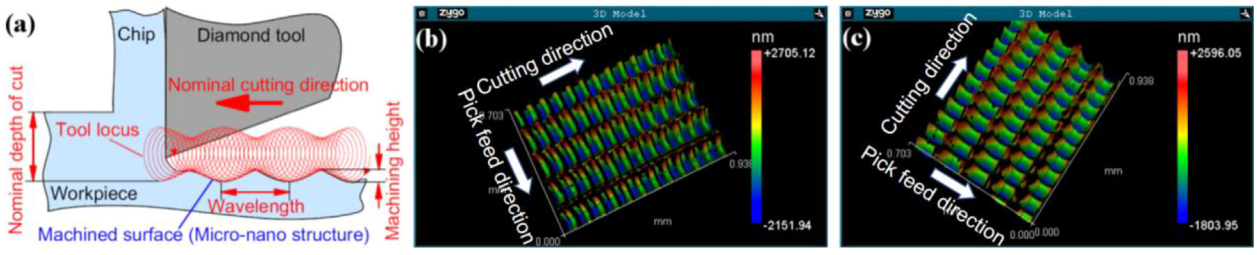

Figure 2. Surface texturing by elliptical vibration diamond cutting. a) Schematic illustration of elliptical vibration cutting; surface textures with different geometries: b) square and c) sinusoid.

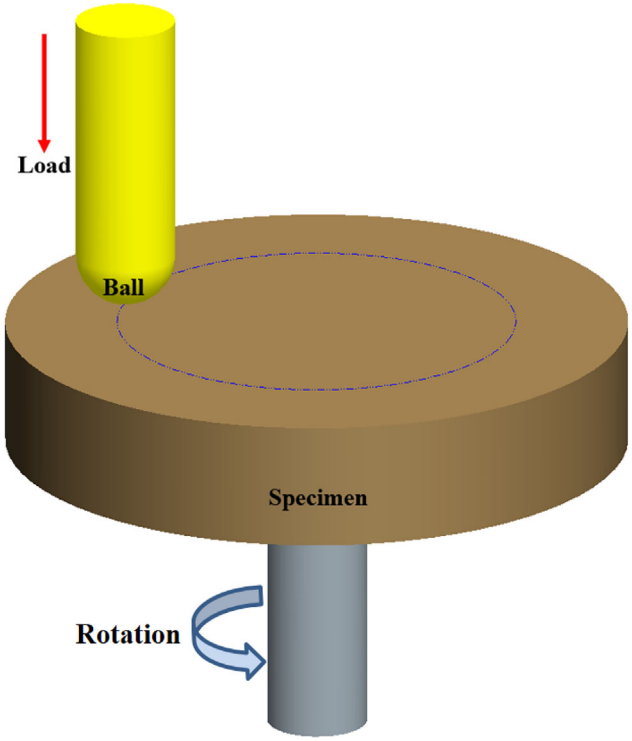

Figure 3. Schematic illustration of the ball-on-disk test.

volume of 3 ml was dropped on the respective surface, which leads to the generation of a stable oil film on the steel surfaces. This procedure was kept constant in order to ensure reproducible testing conditions for all samples. During the tests, no additional oil was supplied to the tribological contact. Due to limited amount of oil given to the tribological contact, it can be assumed that the experiments were performed under starvation. After the friction tests, the specimens were cleaned in an ultrasonic bath with acetone, and then weighted with an electronic balance (accuracy is 0.0001 g) to evaluate the respective mass loss.

3. Results and Discussion

3.1. Textured versus Untextured Specimens

First, friction tests on untextured steel samples using different testing conditions are performed. **Figure 4**a shows the variation of the COF as a function of sliding velocity and normal load for the untextured reference.

As can be seen in Figure 4a, the COF for all experiments conducted under different normal loads or sliding velocities shows a decreasing tendency and is in a range between 0.11 and 0.14. The decreasing trend with increasing sliding velocity is a well-observed phenomenon in tribology and can be correlated with the well-known Stribeck curve. Figure 4b presents the resulting wear scar for the untextured surface after a friction test using a sliding velocity of 15 m min^{-1} and a normal load of 10 N, which shows a pronounced wear scar. The measured values for the COF, the presented wear scar and the slight decrease of the COF with sliding velocity can be well correlated with frictional characteristics typically found under the starved conditions. In addition, the pronounced wear scar implies that a sufficient amount of solid–solid contact was present. This indicates that the experiments were performed under mixed lubrication with a rather high solid–solid contact ratio.

Figure 5a shows the COF of the textured surface with a depth of 13 μm fabricated by laser surface texturing as a function of the applied normal load. The COF of the untextured reference is also presented for comparison. As can be seen in Figure 5a, the COF for the textured surface is significantly reduced for all normal loads. The induced friction reduction can be traced back to a combined effect of different contributions. The surface texturing leads to a reduction of the contact area. Since the contact area is directly proportional to the friction force, this can be directly correlated to the observed reduction in the COF. Due to the experimental conditions of starved lubrication, the rather high solid–solid contact ratio and the observed wear, the generation of wear particles is highly likely. Those wear particles can be effectively trapped in the surface textures thus removing them from the contact zone. Additionally, the surface textures induce a reservoir effect, and oil can be efficiently transported to the contact area once wear has started to occur. Moreover, the surface textures can induce an additional hydrodynamic pressure that may help to improve the frictional behavior, even under severe experimental conditions such as starved conditions. In addition, a certain decrease of the COF with increasing normal load can be observed, similar to the untextured surface. Furthermore, it is worth mentioning that the friction reduction is more pronounced for smaller normal loads. This can be explained by the fact that wear becomes more severe with higher normal load, thus reducing the beneficial effects of surface texturing. Figure 5b shows the COF versus sliding velocity for the laser-textured surface and the reference sample. The friction tests were performed with a constant normal load of 4 N. As can be seen in Figure 5b, the COF of the untextured surface

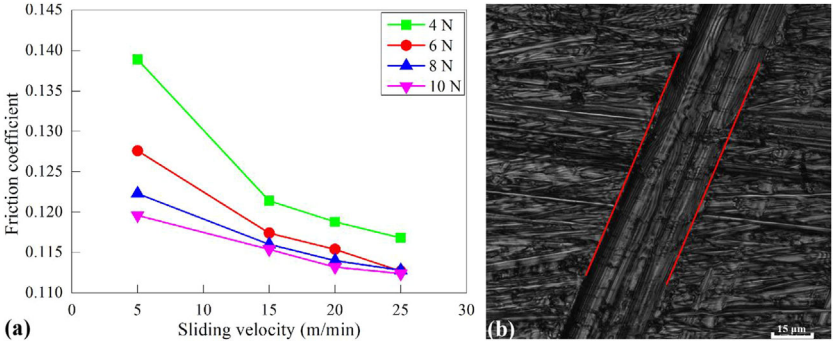

Figure 4. Friction results for the untextured surface. a) COF versus sliding velocity for the untextured surface as a function of the applied normal load and b) resulting wear scar after a friction test using a velocity of 15 m min^{-1} and a normal load of 10 N.

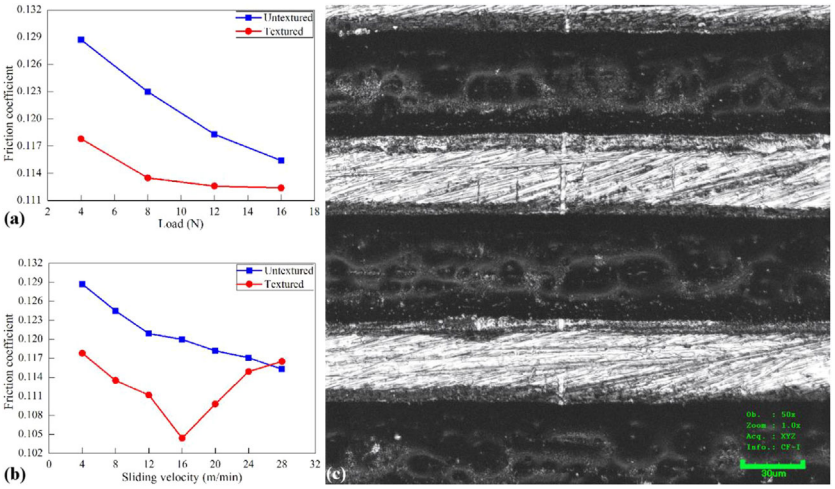

Figure 5. Influence of laser surface texturing (texture depth of 13 μm) on the frictional properties of stainless steel compared to an untextured reference sample. a) COF versus normal load for a sliding velocity of 4 m min^{-1}; b) COF versus sliding velocity for a load of 4 N. c) Resulting wear scar for the textured surface after a sliding test with a sliding velocity of 4 m min^{-1} and a normal load of 4 N.

monotonously decreases with increasing sliding velocity, which can be well correlated with a Stribeck-like behavior. The COF of textured surface first decreases with increasing sliding velocity, reaches a minimum for a sliding velocity of 16 m min^{-1} and then increases again with sliding velocity. In particular, for the largest sliding velocity of 28 m min^{-1}, the COF of the textured surface is slightly higher than the COF of the untextured surface. Similar to Figure 5a, a pronounced friction reduction can be observed, especially for low sliding velocities. Figure 5c reveals the resulting wear of the textured surface after a sliding test with a load of 4 N and a sliding velocity of 4 m min^{-1}, which corresponds to the experimental conditions that yield the highest COF shown in Figure 5a and b. As compared to the pronounced wear scar observed for untextured surface shown in Figure 4b, the induced wear is considerably reduced for the textured surface. Consequently, it can be concluded that the surface textures can help to reduce friction and wear at the same time.

3.2. Effect of Texture Depth

Figure 6 plots the COF versus sliding velocity for the untextured surface and textured surfaces with different texture depths fabricated by laser surface texturing and diamond cutting.

It can be seen that the effect of the surface texturing on the frictional properties is strongly affected by the texture depth and the sliding velocity. The COF for the surface texture with the lowest texture depth of 1.3 μm is higher than that for untextured surface for all the sliding velocities. A possible explanation for this observation is that this depth is not sufficient to store produced wear particles and to produce any additional hydrodynamic pressure build-up. Consequently, the wear particles remain in the contact area and lead to more abrasive wear thus increasing the COF. For texture depths of 8 and 23 μm, the COF is more or less comparable to the COF of the untextured reference. For intermediate texture depths of 13 and 18 μm, a significant friction reduction can be observed. As already mentioned in the Introduction, the induced friction reduction by surface texturing is based upon different mechanisms. It can be assumed that surface textures with intermediate depths can help to build up an additional hydrodynamic pressure and effectively store produced wear particles, which jointly leads to a reduction in the COF. In this context, it needs to be emphasized that there is an important interrelation between the texture depth and the oil film thickness present in the tribological contact. Figure 6 also suggests that there is a critical sliding velocity of 16 m min^{-1} that possesses the most pronounced effect in friction reduction by surface texturing. The maximum friction reduction is about 13% for a texture depth of 13 μm tested under a sliding velocity of 16 m min^{-1} and a normal load of 4 N.

Figure 7 plots the COF versus normal load for the untextured surface and the textured surfaces with different texture depths fabricated by laser surface texturing and diamond cutting. It can be observed from Figure 7 that the COF decreases with increasing normal load, which holds true for all samples. For almost all surface textures, the COF is reduced compared to the COFof the reference surface. Just for the surface texture with the lowest texture depth of 1.3 μm, the COF measured for a normal load of 4 N is slightly higher than that of the reference surface. It can be seen from Figure 7 that the texture depth has a strong impact on the load-dependent friction reduction.

Figure 8 presents the influence of the texture depth on the wear behavior after the frictiontests with a sliding velocity of 16 m min^{-1} and a normal load of 4 N. The wear of the textured surface, as evidenced by the mass loss summarized in Figure 8a, is greatly reduced compared to the untextured surface.

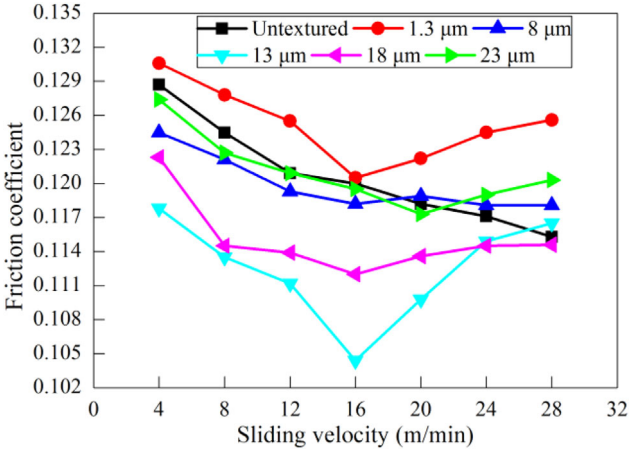

Figure 6. COF versus sliding velocity for the untextured reference and textured samples with different texture depths. The normal load was kept constant at 4 N for all friction tests.

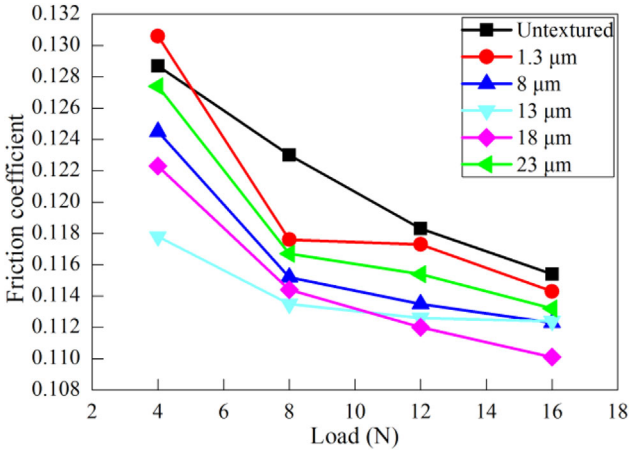

Figure 7. COF versus applied load for textured samples with different texture depths. The friction tests were performed with a sliding velocity of 16 m/min.

Figure 8a also indicates that the minimum mass loss can be found for the textured surface with a texture depth of 13 μm, which goes hand in hand with the maximum friction reduction found for the same surface texture. Figure 8b–f present the worn surface topographies of the textured surfaces with different texture depths. It can be clearly seen that the textured surface with the lowest texture depth of 1.3 μm has the most pronounced wear features, which correlates well with the slightly increased COF observed for this surface texture. The reduced mass loss for the textured surfaces can be well explained by the possible trapping of produced wear particles thus reducing abrasive wear. The analysis of the mass loss correlates well with the results of the COF presented in Figure 6. The maximum reduction in COF and mass loss is found for the surface textures with intermediate texture depths. In contrast, the surface texture with the lowest texture depth shows the highest COF and mass loss, which indicates that the produced wear particles cannot be effectively stored in the surface textures. In addition, for shallow surface textures, it is not possible to build up a sufficiently large additional hydrodynamic pressure to positively influence the tribological properties. On the other hand, deep surface textures (depth of 23 μm) can effectively store the wear particles, but exhibit a rather steep texture geometry. Steep textures lead to undesired edge effects thus increasing the COF and counter balancing the beneficial effects induced by the surface textures. It is also worth to mention that the fluid viscosity has also a strong impact on the texture depth-dependent friction reduction, as the fluid viscosity greatly influences the fluid flow inside the textures and mainly contributes to the hydrodynamic pressure build-up. Furthermore, as compared to additive-free poly-alpha-olefin (PAO) oils, the use of a formulated engine oil with high viscosity can significantly shift the texture-dependent friction reduction.[38] It is planned in a follow-up study to perform experiments with surface textures using PAO oils without any additives and fully formulated oils.

3.3. Effect of Texture Morphology

By diamond turning, two different texture geometries, namely square and sinusoid, were prepared. Subsequent friction tests of those textured surfaces under the same testing conditions were performed to study the influence of the texture geometry on the frictional response.

Figure 9a plots the COF versus sliding velocity for both geometries tested at a normal load of 4 N. It can be seen from

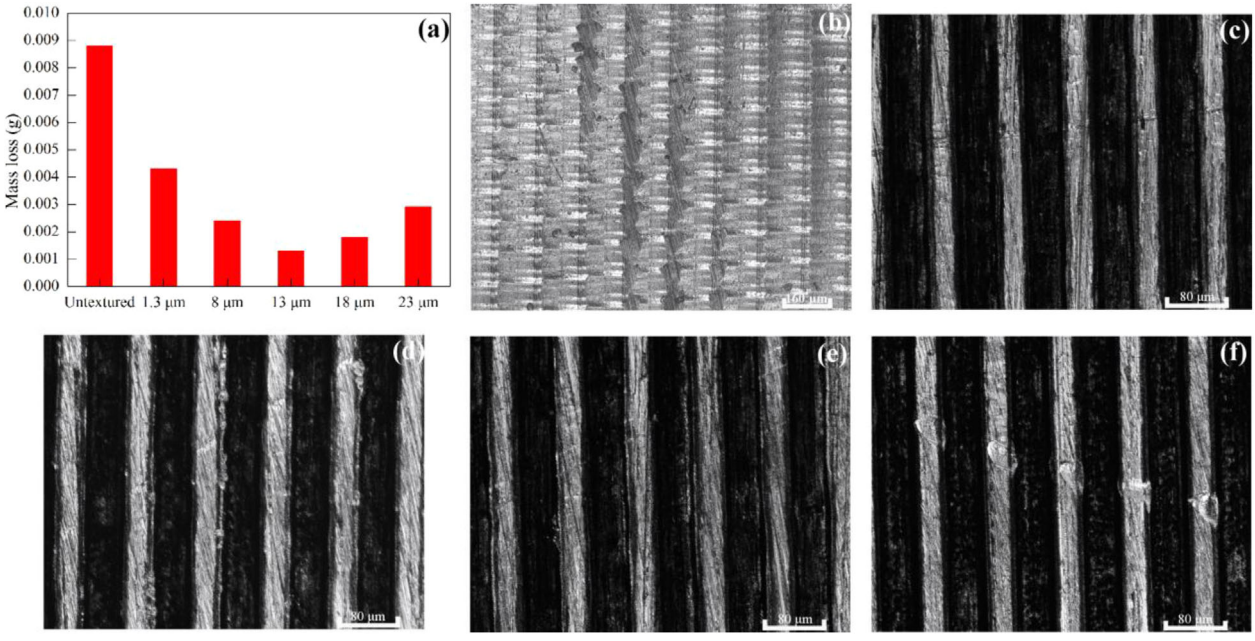

Figure 8. Influence of texture depth on the wear behavior of the textured steel. a) Mass loss; wear morphology for texture depth of b) 1.3 μm, c) 8 μm, d) 13 μm, e) 18 μm, and f) 23 μm.

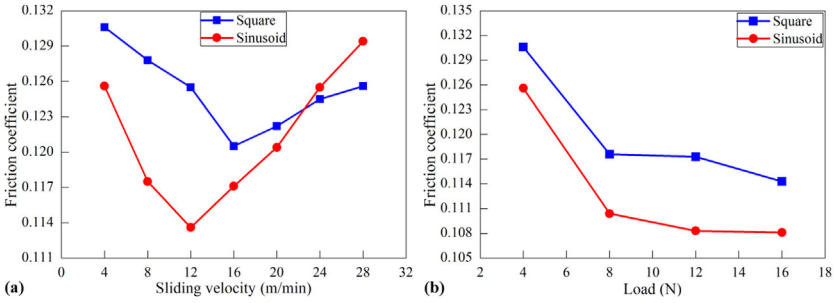

Figure 9. Frictional response of the surface texture with different texture geometries (square and sinusoid).The texture depth was kept constant at 1.3 μm for each texture geometry. COF versus sliding velocity a) and normal load b).

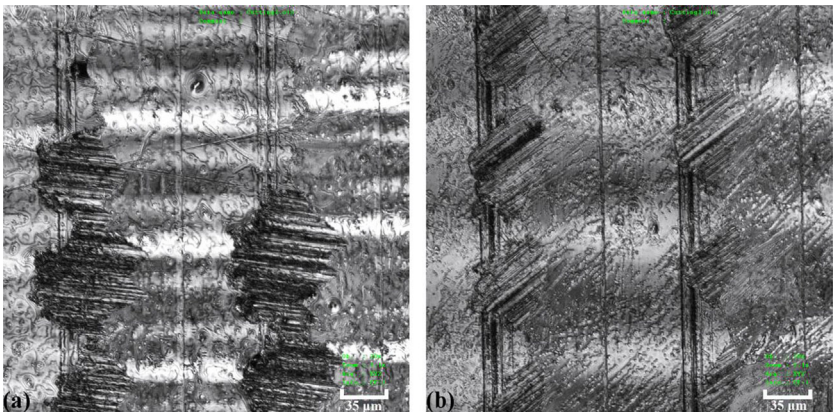

Figure 10. Worn surface topography for the textured surface with a texture depth of 1.3 μm. Texture morphology: square a) and sinusoid b).

Figure 9a that for a sliding velocities smaller than 20 m min^{-1}, the COF of the sinusoid texture is smaller than that of the square one. However, this trend reverses with a further increase in the sliding velocity. Figure 9b plots the COF versus load for both morphologies tested at a sliding velocity of 4 m min^{-1}. As can be seen in Figure 9b, the COF of the sinusoid texture is always smaller compared to that of the square one. This figure also indicates that the texture geometry has a larger influence on the frictional response at a higher load.

Figure 10a and b present the worn surface topographies of the square and sinusoid textures after friction tests with a sliding velocity of 4 m min^{-1} and a normal load of 4 N. It is found that the wear is more pronounced for the square texture compared to that for the sinusoid one, as both extent and depth of wear scar formed on the square texture are higher. This correlates well with the observed friction reduction for the sinusoid geometry compared to that for the square one. The more pronounced wear for the square texturemay generate more wear particles, which significantly contribute to abrasive wear and consequently to an increased COF.

4. Conclusions

Surface textures with different texture depths ranging from 1.3 to 23 μm on stainless steel were fabricated by using laser surface texturing and elliptical vibration diamond cutting. Subsequent ball-on-disk friction tests under starved lubrication show that the presence of the surface textures significantly reduces friction and wear compared to the untextured reference sample. It is also found that the effect of the surface texturing on friction reduction is strongly affected by the texture depth and the testing conditions such as sliding velocity and normal load. Under low normal loads or slow sliding velocities, surface textures with the lowest depth demonstrate a slightly increased COF, whereas textures with intermediate depths show a significant reduction in the COF. It can be assumed that surface textures with intermediate depths can help to build up an additional hydrodynamic pressure and effectively store produced wear particles. Along with the observed friction reduction, the surface textures significantly lower the resulting mass loss. Similar to the observed COF results, surface textures with the lowest depth show a considerably increased mass loss compared to surface textures with intermediate depths that demonstrate the lowest mass loss. Consequently, it could be shown that surface textures with intermediate depths can induce a significant friction and wear reduction at the same time. A clear influence of the texture geometry is verified, that is, the sinusoidal surface texture leads to a reduced COF and less pronounced wear features than the square geometry.

Acknowledgements

The authors greatly acknowledge support from Postdoctoral Scientific Research Development Fund of Heilongjiang Province (LBH-Q16094), the Science and Technology Development Project of Jilin Province (20170520102JH), and the Open Research Foundation of State Key Laboratory of Digital Manufacturing Equipment and Technology in Huazhong University of Science and Technology, China (DMETKF 2018007). A. Rosenkranz gratefully acknowledges the Feodor-Lynen Fellowship provided by the Alexander von Humboldt foundation.

Conflict of Interest

The authors declare no conflict of interest.

Keywords

diamond cutting, friction reduction, laser texturing, surface texturing, texture depth

Received: November 13, 2017
Revised: January 18, 2018
Published online: February 27, 2018

[1] A. Ronen, I. Etsion, Y. Kligerman, *Tribol. T.* **2001**, *44*, 359.
[2] U. Pettersson, S. Jacobson, *Tribol. Int.* **2003**, *36*, 857.
[3] G. Stachowiak, P. Podsiadlo, *Tribol. Lett.* **2008**, *32*, 13.
[4] Y. L. Zhang, X. G. Zhang, T. H. Wu, Y. B. Xie, *Ind. Lubr. Tribol.* **2016**, *68*, 158.
[5] W. Wei, T. M. Shao, G. M. Chen, *Sci. China Technol. Sci.* **2016**, *59*, 183.
[6] A. Rosenkranz, T. Heib, C. Gachot, F. Mücklich, *Wear* **2015**, *334*, 1.
[7] A. Rosenkranz, L. Reinert, C. Gachot, F. Mücklich, *Wear* **2014**, *318*, 49.
[8] C. Gachot, A. Rosenkranz, L. Reinert, E. Ramos-Moore, N. Souza, M. H. Müser, F. Mücklich, *Tribol. Lett.* **2013**, *49*, 193.
[9] C. Caciu, E. Decenciere, D. Jeulin, *Tribol. T.* **2008**, *51*, 533.
[10] H. Ogawa, S. Sasaki, A. Korenaga, K. Miyake, M. Nakano, T. Murakami, *Proc. Inst. Mech. Eng. J. J. Eng. Tribol.* **2010**, *224*, 885.
[11] C. X. Gu, X. H. Meng, Y. B. Xie, Y. M. Yang, *Tribol. Int.* **2016**, *94*, 591.
[12] S. M. Hus, Y. Jing, F. Zhao, *Surf. Topogr. Metrol. Prop.* **2016**, *4*, 014004.
[13] C. Gachot, A. Rosenkranz, S. M. Hsu, H. L. Costa, *Wear* **2017**, *372–373*, 21.
[14] M. Sedlacek, B. Podgornik, A. Ramalho, D. Cesnik, *Tribol. Int.* **2017**, *115*, 268.
[15] S. M. Hsu, Y. Jing, D. Hua, H. Zhang, *J. Phys. D Appl. Phys.* **2014**, *47*, 335307.
[16] J. W. Byun, H. S. Shin, M. H. Kwon, B. H. Kim, C. N. Chu, *Int. J. Precis. Eng. Manuf.* **2010**, *11*, 747.
[17] J. G. Parreira, C. A. Gallo, H. L. Costa, *Surf. Coat. Tech.* **2012**, *212*, 1.
[18] L. R. R. da Silva, H. L. Costa, *Wear* **2017**, *376–377*, 1601.
[19] N. Moronuki, Y. Furukawa, *CIRP Ann. Manuf. Technol.* **2003**, *52*, 471.
[20] I. Etsion, *J. Tribol. Trans. ASME* **2005**, *127*, 248.
[21] A. Kovalchenko, O. Ajayi, A. Erdemir, G. Fenske, I. Etsion, *Tribol. Int.* **2005**, *38*, 219.
[22] Y. Q. Xing, J. X. Deng, X. T. Feng, S. Yu, *Mater. Des.* **2013**, *52*, 234.
[23] D. Kim, J. La, S. M. Kim, S. Y. Lee, *Mater. Res. Bull.* **2014**, *58*, 39.
[24] A. Rosenkranz, J. C. Pangraz, C. Gachot, F. Mucklich, *Wear* **2016**, *368*, 350.
[25] M. Wakuda, Y. Yamauchi, S. Kanzaki, Y. Yasuda, *Wear* **2003**, *254*, 356.
[26] W. Tang, Y. K. Zhou, H. Zhu, H. F. Yang, *Appl. Surf. Sci.* **2013**, *273*, 199.
[27] J. L. Mo, Z. G. Wang, G. X. Chen, T. M. Shao, M. H. Zhu, Z. R. Zhou, *Wear* **2013**, *301*, 671.
[28] L. M. Vilhena, A. Ramalho, A. Cavaleiro, *Lubr. Sci.* **2017**, *29*, 493.
[29] A. Rosenkranz, A. Szurdak, C. Gachot, G. Hirt, F. Mucklich, *Tribol. Int.* **2016**, *95*, 290.
[30] M. H. Cho, S. Park, *Tribol. Int.* **2011**, *44*, 859.
[31] Y. He, Y. D. Yan, Y. Q. Geng, E. Brousseau, *Appl. Surf. Sci.* **2018**, *427*, 1076.
[32] A. Arslan, H. H. Masjuki, M. A. Kalam, M. Varman, R. A. Mufti, M. H. Mosarof, L. S. Khuong, M. M. Quazi, *Crit. Rev. Solid State Ma. Sci.* **2016**, *41*, 447.
[33] C. Flucke, R. Glabe, E. Brinksmeier, *Ind. Diam. Rev.* **2007**, *67*, 25.
[34] J. W. Yan, T. Oowada, T. F. Zhou, T. Kuriyagawa, *J. Mater. Process. Technol.* **2009**, *209*, 4802.
[35] Y. L. Chen, Y. D. Cai, Y. Shimizu, S. Ito, W. Gao, B. F. Ju, *J. Micromech. Microeng.* **2015**, *26*, 025002.
[36] J. G. Zhang, N. Suzuki, Y. L. Wang, E. Shamoto, *Precis. Eng.* **2015**, *39*, 86.
[37] J. G. Zhang, J. J. Zhang, T. Cui, Z. W. Hao, A. A. Zahrani, *J. Manuf. Process.* **2017**, *29*, 389.
[38] D. Braun, C. Greiner, J. Schneider, P. Gumbsch, *Tribol. Int.* **2014**, *77*, 142.

